Research Square

Preprints are preliminary reports that have not undergone peer review.
They should not be considered conclusive, used to inform clinical practice,
or referenced by the media as validated information.

Substrate stiffness regulates human vaginal fibroblast activation and extracellular matrix remodeling

Temitope Obisesan

teo23@pitt.edu

University of Pittsburgh https://orcid.org/0009-0008-8538-3739

Jingnan Ye

Carnegie Mellon University

Mya Fulton

University of Pittsburgh

Marrisa Therriault

University of Pittsburgh

Katrina Knight

University of Pittsburgh

Leslie Meyn

University of Pittsburgh

Yu Li Wang

Carnegie Mellon University

Pamela Moalli

University of Pittsburgh

Research Article

Keywords: pelvic organ prolapse, click chemistry, substrate stiffness, polyacrylamide gel, mechanotransduction, myofibroblasts, integrins

Posted Date: November 19th, 2026

DOI: https://doi.org/10.21203/rs.3.rs-11776457/v1

License: This work is licensed under a Creative Commons Attribution 4.0 International License.
Read Full License

Additional Declarations: The authors declare no competing interests.

Abstract

Pelvic organ prolapse (POP) involves mechanical failure of the vagina and its supporting tissues. Polypropylene mesh used in surgical repair can create a mechanical environment that differs substantially from native tissue and is associated with maladaptive remodeling. However, the stiffness-dependent responses of vaginal fibroblasts remain unclear. We hypothesized that increasing substrate stiffness would promote myofibroblast differentiation and matrix deposition, whereas substrates approximating vaginal tissue stiffness would support a less activated phenotype. Primary human vaginal fibroblasts from three premenopausal donors without prolapse were cultured on gelatinfunctionalized polyacrylamide hydrogels of 5, 8, and 20 kPa for 1, 3, and 7 days. Outcomes included viability, myofibroblast differentiation, α5 integrin expression, collagen deposition, MMP-2 activity, traction force, TGF-β1 secretion, and YAP localization. Viability remained ≥ 98% across conditions. Myofibroblast density increased over time and was greater on 20kPa than 5 kPa substrates, although myofibroblast proportions did not differ significantly among hydrogel stiffnesses. The stiffest hydrogels supported the greatest collagen deposition and active MMP-2 levels, while cell mediated traction force increased progressively with stiffness. Traction force peaked at day 1, preceding later myofibroblast accumulation and collagen deposition. Early YAP nuclear localization was greater on higher-stiffness substrates and returned toward baseline by days 3–7. Active TGF-β1 remained below detection despite increasing total TGF-β1 over time. These data show that substrate stiffness regulates human vaginal fibroblast activation and matrix remodeling through distinct temporal responses, providing an experimental foundation for matching mechanical properties of biomaterials to the vagina for pelvic floor repair.

INTRODUCTION

Pelvic organ prolapse (POP) involves maladaptive remodeling of the vagina and its supporting tissues, leading to compromised pelvic support [1, 2]. Approximately 12.6% of women in the United States undergo surgery for POP by age 80 [3]. Polypropylene mesh (PPM) is commonly used to reinforce prolapse repairs. PPM has a much higher modulus than vaginal tissue [4, 5, 6] and a mismatch between mesh and tissue mechanics has been proposed as one contributor to adverse host responses [4, 7]. In macaques, implantation of high-stiffness mesh was associated with reduced vaginal smooth muscle and collagen content and increased collagenase activity [8], as well as reduced vaginal contractile function [9]. Deformed mesh configurations were also associated with vaginal thinning, mesh exposure, and regional myofibroblast proliferation and fibrosis [10]. These findings link mesh mechanics with vaginal tissue response, but they leave open how stiffness, independent of other mesh properties, affect fibroblasts' behavior.

Fibroblasts synthesize, organize, and remodel the extracellular matrix (ECM), thereby regulating cell differentiation, tissue structure and mechanics. As sentinel cells, fibroblasts are highly responsive to mechanical cues triggered by altered matrix stiffness which, in turn, influences their transition into pro-fibrotic myofibroblast phenotypes through a process known as the fibroblast-to-myofibroblast transition (FMT). This transition is marked by the upregulation of α-smooth muscle actin (α-SMA), formation of

contractile actin stress fibers which place traction on the wound, and the synthesis of a provisional matrix rich in collagen which are all necessary for wound healing and closure [11, 12, 13, 14]. Once the appropriate matrix stiffness and wound closure have been achieved, these cells disappear in a wave of apoptosis [15]. Persistent mechanical signals or chemical cues can impair resolution resulting in a sustained myofibroblast response with pathological matrix deposition and impaired tissue function [16]. Substrate stiffness is one of the principal regulators of fibroblast phenotype, with increased matrix rigidity inducing myofibroblast differentiation, upregulation of α-SMA, and increased collagen synthesis in dermal, cardiac, and pulmonary fibroblasts [17, 18]. Vaginal tissue studies have reported differences in stiffness between prolapsed and healthy tissue, and in vitro studies have linked substrate stiffness to myofibroblast markers, integrin expression, and matrix production in vaginal fibroblasts [14, 19, 20]. How human vaginal fibroblasts progress through FMT over time across defined substrate stiffnesses, and how that progression relates to mechanosensitivity and matrix remodeling, remains unclear.

Tunable synthetic hydrogels, like polyacrylamide gels, provide a means to study fibroblast responses across controlled substrate stiffnesses and as such provide insight into mechanical regulation of stiffness induced FMT and ECM remodeling [21, 22]. We used PA hydrogels of 5, 8, and 20 kPa, spanning soft, healthy reproductive age vaginal ECM, and a fibrotic ECM [19]. We used primary vaginal fibroblasts isolated from young premenopausal women without POP to characterize mechanosensitive responses. We aimed to provide insight into the spatially variable vaginal tissue responses observed when mesh is loaded [10]. At days 1, 3, and 7, we measured fibroblast and myofibroblast populations, mechanotransduction responses (α5-integrin, YAP localization, traction force), and matrix remodeling (collagen deposition, MMP activity, TGF-β1). We hypothesized that increasing substrate stiffness would promote fibroblast activation, progressive myofibroblast transition, increased traction force, and increased matrix deposition, whereas gels approximating the stiffness of vaginal tissue would maintain a less activated state. Using premenopausal fibroblasts without POP defines these responses under normal conditions and provides a baseline for future comparisons with fibroblasts from menopausal women and women with POP.

2. MATERIALS AND METHODS

2.1 Development of in vitro model

A custom in vitro biochamber was constructed using a 70 × 50 × 3-mm Plexiglass plate with an approximate bored annulus of 35mm diameter at the center. A large (50mm x 75mm x 1mm thick) microscope glass slide (12-550C, Fisher Scientific, Waltham, MA) was sealed to the underside of the plate using vacuum grease (Dow Corning). The microscope glass slides were flame-activated and treated with bind-silane working solution (mix of 95% ethanol, 5%(v/v) acetic acid, and 0.3% (v/v) bind-silane) to facilitate hydrogel anchoring. Circular 25mm coverslips (22038999, Fisher Scientific, Waltham, MA) were treated with RainX (ITW Global Brands, Houston TX) to create a hydrophobic surface facilitating gel detachment after polymerization. This setup allowed hydrogel polymerization and subsequent cell culture within the defined central region. For most downstream experiments including

immunofluorescence (IF), cell viability, and Picro Sirius Red staining, biochambers with a 20 mm diameter annulus were used to confine the gel. In contrast, 35 mm diameter chambers were used for traction force microscopy (TFM) to provide a larger surface area for defining substrate traction induced by individual fibroblast cells. The 35 mm diameter biochambers were also used for matrix metalloproteinase (MMP) gelatin zymography and TGFβ-1 ELISA experiments to enable the collection of a larger volume of conditioned media, which was necessary for both sufficient protein detection and repeatability.

2.2 Polyacrylamide Hydrogel Preparation and Functionalization (fPAGs)

Polyacrylamide (PA) precursor solutions were prepared in deionized water using 40% w/v acrylamide and 2% w/v N,N' methylenebisacrylamide (Bio-Rad, Hercules, CA), at concentrations corresponding to target elastic moduli of 5kPa (5% acrylamide, 0.15% bisacrylamide), 8kPa (5% acrylamide, 0.3% bis-acrylamide), and 20kPa (8% acrylamide,

0.264% bis acrylamide) as previously characterized through atomic force microscopy (AFM)[23]. The stiffness range was selected to compare a lower-stiffness condition with a substrate near the reported modulus of healthy vaginal extracellular matrix (8.9 ± 4.26 kPa), and to test fibroblast responses to a higher-stiffness condition. For context, prolapsed vaginal extracellular matrix has been reported to have an effective modulus of 11.2 ± 5.37 kPa; thus, 20 kPa was used as an elevated-stiffness challenge. Prior work also found stiffness-associated changes in vaginal fibroblast alpha smooth muscle actin (α-SMA) expression, supporting the relevance of testing stiffness-dependent responses in this range [10]. For a positive high stiffness control, we used plain glass slides. To each formulation, 2 µL of propargyl acrylate per mL of precursor solution was added to introduce alkyne functional groups for subsequent click chemistry. Lithium phenyl-2,4,6 trimethylbenzoylphosphinate (LAP) was added as a photoinitiator at a final concentration of 2 mg/mL. A fixed volume of 120 µL of the hydrogel precursor solution was polymerized under 365 nm UV light for 10 minutes between the activated glass slide and Rain-X coverslips. After polymerization, the coverslips were carefully removed by submerging the PA gels in DI water. Following polymerization, the alkyne-functionalized polyacrylamide (PA) gels were rinsed with 50 mM HEPES buffer (pH 8.5) for 15 minutes to remove unreacted monomers and condition the surface. Gelatin-azide was then covalently conjugated to the gels to facilitate cell adhesion via copper-catalyzed azide-alkyne cycloaddition (CuAAC) click chemistry (Fig. 1), following the method outlined by Hong et al. (2010) [24].

2.3 Primary human vaginal fibroblast (hvFs) culture

A full-thickness vaginal punch biopsy (N = 3) was obtained from premenopausal women without prolapse as part of the Magee-Womens Research Institute Pelvic Floor Tissue Biorepository (IRB: CR19080175-010). Tissue samples were minced into small pieces and plated into 6-well plates (Catalog no.: 150628, Thermo Fisher Scientific, Waltham,

MA) until the human vaginal fibroblasts HvFs) that exited the tissue achieved confluence. Cells were maintained in supplemented DMEM (Dulbecco's Modified Eagle Medium (DMEM), 14% Fetal Bovine Serum (FBS), 1.5% Amphotericin B, 1% Pen Strep) at 37°C in humidified 5% CO_2. Adherent HvFs were expanded, with medium changes every 2–3 days. At passage 5, HvFs (N = 3) were seeded onto PA gels (n = 2 replicates) or plain glass slides as positive controls, and cultured for 1, 3, and 7 days for downstream analyses. For immunofluorescence, cell viability, and Picro Sirius Red staining, the cells were seeded at a density of 96 cells/mm² and cultured in DMEM supplemented with 14% FBS, 1.5% Amphotericin B, and 1% Pen-Strep to promote cell attachment and spreading. For gelatin zymography, the HvFs were cultured in phenol-free DMEM, serum free media consisting of 0.2% lactalbuminhydrosylate, 1% Insulin-Transferrin-Selenium (ITS-G), 1% Amphotericin B, and 0.1% Pen-Strep in order to minimize serum-derived protease activity and optimize detection of cell secreted MMPs. For traction force microscopy, cells were seeded on 25 mm PA gels at density 10.2 cells/mm², 6.1 cells/mm², 2.0 cell/mm², and 1 cells/mm², and cultured for 1, 3, and 7 days respectively prior to traction force analysis, ensuring sparse distribution for the quantification of single cell traction forces. All cell lines used for this study (N = 3) were derived from pre-menopausal patients with no hormone use and no diagnosis of pelvic organ prolapse.

2.4 Cell Viability

C ell viability was assessed in all PA gel conditions using the LIVE/DEAD Cell Viability/Cytotoxicity Kit (L3224, Thermo Fisher Scientific, Waltham, MA), utilizing calceinAM and ethidium homodimer-1. According to the manufacturer's instructions [25], adherent hvFs were rinsed with PBS and incubated with staining solution containing 2μM calcein AM and 4μM ethidium homodimer-1 for 30 minutes at room temperature, protected from light. Calcein AM is a non-fluorescent, cell-permeant dye that is converted by intracellular esterases into calcein, producing green fluorescence in live cells with intact membranes. Ethidium homodimer-1 is excluded by intact cell membranes but enters cells with compromised membranes, binding to nucleic acids and producing red fluorescence in dead cells. Heat killed cells were used as a positive control for non-viable cells. Stained cells were visualized by fluorescence microscopy. The numbers of live (green, calcein positive) and dead (red, ethidium homodimer-1–positive) cells were quantified in at least five randomly chosen 20X fields per sample, and viability was expressed as the percentage of live cells relative to the total number of cells.

2.5 Immunofluorescence

2.5.1 Immunofluorescence for fibroblast-to-myofibroblast transition and integrin acquisition

To assess cytoskeletal remodeling and mechanosensitive protein expression, immunofluorescence staining was performed on HvFs cultured on polyacrylamide gels for 1, 3, and 7 days. Cells were fixed with 4% paraformaldehyde for 20 minutes at room temperature and blocked with 2% donkey serum/2.5% normal horse serum (s-2012-50 Newark, CA) for 1 hour to prevent non-specific binding. Primary antibodies against αsmooth muscle actin (α-SMA) - a marker of myofibroblast differentiation (2798495,

Invitrogen, Carlsbad, CA), vimentin - a mesenchymal intermediate filament protein (NB300-223, Novus Bio. Centennial, CO), and integrin α5β1 - a key mechanoreceptor mediating ECM adhesion and stiffness sensing (ab150361 Abcam, Waltham, MA) were applied for overnight incubation at 4°C at a dilution of 1:200. After thorough washing, cells were incubated with Alexa Fluor™ Plus 594 (A32744 Invitrogen, Carlsbad, CA), Alexa Fluor 647 (A78952 Invitrogen, Carlsbad, CA), and Alexa Fluor 488 (15077, Abcam, Waltham, MA) at a concentration of 1:200 for 1 hour at room temperature. Samples were mounted with a DAPI-containing antifade reagent (Vectashield, Vector Laboratories, Newark, VA, USA) to visualize cell nuclei. At 20X magnification using a Nikon confocal microscope (Melville, NY), five 3 x 3 non-overlapping regions spanning the entire gel area were acquired per sample. Quantitative analysis of fluorescence intensity compared to negative (primary delete) controls, and positive cell counts were done using QuPath software, enabling comparative assessment of fibroblast-to-myofibroblast transition and integrin-mediated mechanotransduction.

2.5.2 Immunofluorescence for YAP nuclear translocation and TGFβR1 expression

To assess mechanotransduction signaling, HvFs cultured on fPAGs and PGs at days 1, 3, and 7 were additionally stained for Yes-associated protein (YAP), a transcriptional coactivator whose nuclear translocation reflects mechanosensitive signaling, and transforming growth factor-β receptor 1 (TGFβR1), to confirm receptor availability for TGF-β1 signaling. Following the fixation and blocking protocol described above (Section 2.5.1), primary antibodies against YAP (sc-101199, Santa Cruz Biotechnology, Dallas, TX) and TGFβR1 (PA5-98192, Thermo Fisher Scientific, Waltham, MA) were applied overnight at 4°C at a dilution of 1:200. Following washing, cells were incubated with Alexa Fluor™ Plus 594 (A32744 Invitrogen, Carlsbad, CA) and Alexa Fluor 488 (15077, Abcam, Waltham, MA) at a concentration of 1:200 for 1 hour at room temperature together with Alexa Fluor 647 Phalloidin (A22287, Thermo Fisher Scientific, Waltham, MA) to visualize the actin cytoskeleton and define cell boundaries. Nuclei were visualized with DAPIcontaining antifade mounting medium (Vectashield, Vector Laboratories, Newark, CA). Images were acquired at 20X magnification as described in section 2.5.1 and YAP nuclear-to-cytoplasmic (N/C) intensity ratio was quantified in QuPath by defining nuclear regions using DAPI staining and cytoplasmic regions using phalloidin-defined cell boundaries, with the ratio calculated as mean YAP fluorescence intensity in the nuclear region divided by mean intensity in the cytoplasmic region per cell.

2.6 Picrosirius red stain

HvFs cultured on the PA gels were rinsed with 1X PBS and fixed with 4% paraformaldehyde for 20 minutes at room temperature. Following fixation, gels were rinsed in DI water and stained in Picrosirius Red solution for 1 hour at room temperature with gentle agitation. Picrosirius Red solution was prepared by dissolving Direct Red 80 (365548, Sigma Aldrich, Darmstadt, Germany) in saturated aqueous picric acid (5860-16, Ricca Chemical, Arlington, TX, USA) to yield a final concentration of 0.145mM. After staining, gels were briefly decolorized in acetic acid water (1:2 glacial acetic acid to DI H_2O) for 10 seconds to remove nonspecific background. Samples were then dehydrated sequentially in 95% ethanol

once and twice in 100% ethanol, followed by clearing in xylenes three times, for 1 minute each. Images were acquired using a Nikon ECLIPSE 90i upright microscope (Nikon USA, Melville, NY) under polarized light at 10X magnification. Collagen fiber deposition was quantified by color segmentation of red versus green/yellow pixels using MATLAB code previously developed in prior work [10].

2.7 Gelatin zymography

Conditioned media was collected from HvFs cultured on hydrogels on days 1, 3, and 7, centrifuged to remove cellular debris, and stored at -80°C until analysis. The protein concentration of each sample was measured using a DC protein assay (5000114, Biorad, Hercules, CA). Substrate zymography with 500ng protein from each conditioned media sample was mixed with novex Tris-Glycine SDS non-reducing sample Buffer (LC2676 Invitrogen, Carlsbad, CA) and loaded onto pre-cast 10% gelatin zymogram gels (EC61752 Invitrogen, Carlsbad, CA). Gels were initially run at 60 V for 20 minutes to stack the protein, followed by separation at 125 V for 1.5 hours. Experiments were carried out in duplicates as described previously [26, 27] with the inclusion of MMP-9 standard (92kDa) on each gel to normalize variations between gels. Gel images were acquired using a Bio-Rad ChemiDoc EZ Imaging System (Bio-Rad Laboratories, Hercules, CA, USA) and analyzed with ImageJ. The intensities of the bands were quantified and normalized to the MMP-9 standard as well as to total protein concentration in the respective samples.

2.8 TGF-β1 quantification

TGF-β1 levels were quantified in conditioned media using a commercially available enzyme-linked immunosorbent assay (DB100C ELISA; R&D Systems, Minneapolis, MN), following the manufacturer's protocol. Total protein was measured using the DC Protein Assay Kit (catalog nos. 5000113, 5000114, and 5000115; Bio-Rad, Hercules, CA), and samples were normalized to 40 µg protein per well. To measure total TGF-β1, samples were acid-activated and neutralized according to the manufacturer's protocol. Standards spanning 31.3–2,000 pg/mL were used, with calibrator diluent as the zero standard. Conditioned medium from cells known to produce TGF-β served as a positive control. Samples were assayed in duplicate. Absorbance was measured at 470 nm, using 540 nm as the reference wavelength to correct for background and optical variation.

2.9 Traction force microscopy

Polyacrylamide substrates for traction force microscopy (TFM) were fabricated following established protocols [23]. Briefly, polyacrylamide solutions of varying concentrations were prepared to achieve substrates of different stiffness values, as described above. A 20µL droplet of the solution was pipetted onto a bind-silane-treated glass substrate and overlaid with a 25 mm diameter circular glass coverslip. After polymerization, the coverslip was removed, and a second 20µL droplet of the same PA solution containing 0.1% v/v fluorescent beads (0.5µm diameter, Molecular Probes, Eugene, OR) was added on top of the first gel layer. Another 25 mm circular coverslip was placed on top, and the assembly was centrifuged upside down at 300 × g for 5 minutes to localize the beads near the gel surface. Substrates were then functionalized as described above.

To measure substrate displacements caused by cellular traction forces, isolated human vaginal fibroblasts (HvFs) were seeded onto the PA substrates on day 0 and cultured for 1, 3, and 7 days. Fluorescent bead images were captured before and after cell removal using 1 mL of 0.5% Trypsin-EDTA (Thermo Fisher Scientific, Waltham, MA). Imaging was performed on a Nikon Eclipse Ti microscope equipped with a dry 40×/NA 0.75 Plan Fluor phase-contrast objective and a Photometrics Prime 95B CMOS camera (1200 × 1200 pixels, Tucson, AZ). At this magnification, each pixel represents an area of 0.275 × 0.275 μm².

Bead images were processed to compute cell-substrate traction force. Briefly, displacement fields were calculated from paired images (before and after cell detachment) using an iterative particle image velocimetry (PIV) plugin in ImageJ. The displacement vectors were then used to compute traction force maps in MATLAB 2023a (The MathWorks, Natick, MA) using a deep learning-based TFM model developed in previous work [28]. Only vectors within the segmented cell boundary were used to compute the root mean square (RMS) traction force. Cell area was measured using ImageJ.

Statistical analysis

Preliminary data showed that 92.2% of myofibroblasts cultured on plain glass expressed integrins (SD, 9.7%). Assuming a correlation of 0.4 among repeated measurements within donors, repeated-measures analysis of variance indicated that three donors would provide 80% power to detect a difference across four stiffness levels, assuming an effect size of 2 and a significance level of 0.05. Differences in myofibroblast differentiation, collagen deposition, TGF-β levels, traction force, and MMP activity by day and stiffness were assessed using mixed-effects general linear models. Pairwise comparisons were conducted using post-estimation contrasts of model coefficients, with statistical inference based on z statistics. Analyses were performed using Stata 19 (StataCorp LLC, College Station, TX), with $p < 0.05$ considered statistically significant.

3. RESULTS

3.1 Functionalized polyacrylamide gels support human vaginal fibroblasts (HvFs) viability across stiffnesses

To evaluate cytocompatibility across substrates, cell viability was assessed using LIVE/DEAD Cell Viability/Cytotoxicity Kit (L3224, Thermo Fisher Scientific, Waltham, MA), on gelatin-functionalized polyacrylamide gels (fPAGs) with varying stiffnesses (5kPa, 8kPa, 20kPa/N = 3 per stiffness in duplicates) and on plain glass (positive control/N = 3). Figure 2a, b shows that cell viability remained high across all substrate stiffnesses and culture time points with ≥ 98% (0.001) viability observed 24 hours after seeding. Among the fPAGs, viability was 0.2% higher on 8kPa compared to the 5kPa fPAG ($p < 0.001$) (Table 1). These results indicate that functionalized gels across all substrate stiffnesses and time points support robust fibroblast survival and do not elicit cytotoxic effects.

3.2 Matrix stiffness influences human vaginal fibroblast to myofibroblast transition over time

To quantify the human vaginal fibroblast-to-myofibroblast transition, fibroblasts were defined as DAPI+ / Vimentin+/αSMA- cells and myofibroblasts as DAPI+ / Vimentin+/aSMA+ cells following the acquisition of alpha smooth muscle actin (α-SMA) stress fibers (Fig. 3a). Cell density and relative proportions were evaluated on functionalized polyacrylamide gels (fPAGs) of increasing stiffness (5, 8, and 20kPa) and plain glass slide (PGs) at days 1, 3, and 7. Fibroblast density remained stable throughout the 7 days of cell culture. Compared with day 1, fibroblast density did not differ on day 3 ($p = 0.165$) or day 7 ($p = 0.128$), and no difference was observed between days 3 and 7 ($p = 0.989$). Likewise, fibroblast density did not differ when compared to the PGs and among substrate stiffnesses (5, 8, and 20 kPa fPAGs - all $p > 0.05$; Fig. 3b, Table 2). Myofibroblast density, in contrast, increased significantly over time. Relative to day 1, myofibroblast density increased by 1,355 cells/mm² on day 3 and by 5,474 cells/mm² on day 7 (both $p < 0.001$); these densities were 2.24 and 6.01 times the day 1 level, respectively. Myofibroblast density was 2.68 times as high on day 7 as on day 3 ($p = 0.004$). In comparison with PG, myofibroblast density was significantly lower on 5kPa and 20kPa fPAGs ($p < 0.001$) while no difference was observed on 8kPa ($p = 0.393$). Among the fPAGs, myofibroblast density was 1.6 times higher on 20kPa than on 5kPa ($p < 0.001$) with no differences between 5 and 8kPa or between 8 and 20kPa (Fig. 3c, Table 2). The relative proportions of fibroblasts and myofibroblasts demonstrated a shift in cell phenotype over time. Fibroblast and myofibroblast percentages did not differ significantly between days 1 and 3 or between days 1 and 7 (all $p > 0.05$). However, between days 3 and 7, overall fibroblast percentage decreased by 13.5%, with a corresponding 13.5% increase in myofibroblast percentage ($p < 0.001$). Relative to PG, 8kPa fPAGs had 4.1% more fibroblasts and a corresponding 4.1% fewer myofibroblasts (both $p = 0.042$), with no difference observed on 5 or 20kPa fPAGs or among the fPAGs stiffnesses themselves (Fig. 3d, Table 2).

3.3 Matrix stiffness regulates α5 integrin acquisition over time

To further evaluate the activation of fibroblasts and their transition to myofibroblasts, we assessed the expression of alpha 5 (α5) integrin, a mechanosensitive adhesion receptor involved in cell-extracellular matrix interactions and implicated in fibroblast activation. Because the polyacrylamide gels were functionalized with gelatin, its receptor, α5 integrin was quantified to determine how matrix stiffness influences integrin-mediated cell adhesion during fibroblast activation. α5 integrin-positive cell density, relative proportions and co-localization of α5 integrin with alpha smooth muscle actin (α SMA) and vimentin positive cells were quantified across time and fPAGs substrate stiffnesses. (Fig. 4a). Overall, we observed α5 integrin-positive cell density increased significantly over time. Relative to day 1, α5 integrin positive cell density increased by X% at day 3 ($p < 0.001$) and by X% at day 7 ($p < 0.001$). The integrin-positive cell density on day 7 was over two times as high as day 3 ($p = 0.046$). Compared with PG, α5 integrin-positive cell density was lower on 5kPa ($p < 0.001$), 8kPa ($p = 0.007$), and 20kPa ($p <$

0.001) fPAGs. Among the fPAGs, α5 integrin-positive cell density was lower on 5kPa than on 8kPa ($p < 0.001$) and 20kPa ($p = 0.002$), with no difference observed between 8 and 20kPa ($p = 0.306$). The proportion of α5 integrin-positive cells remained stable over time, with no significant differences between days 1 and 3 ($p = 0.085$), days 1 and 7 ($p = 0.446$), or days 3 and 7 ($p = 0.065$). Across substrate stiffnesses, however, the proportion of α5 integrin-positive cells was lower on 5kPa ($p < 0.001$), 8kPa ($p = 0.033$), and 20kPa ($p < 0.001$) than on PGs. Among the fPAGs, 20 kPa exhibited a higher proportion of α5 integrin-positive cells than 5kPa ($p < 0.001$) with no differences observed between 5 and 8 kPa or between 8 and 20kPa (Table 3). This pattern diverged when fibroblasts and myofibroblasts were considered separately. The proportion of α5 integrin positive fibroblasts did not change over time (all $p > 0.05$; Fig. 4b, 4d) and was 13% lower on 5kPa fPAG than on PGs ($p < 0.001$), 18% lower on the 8kPa ($p = 0.028$), and 3% lower on the 20kPa ($p < 0.001$) fPAGs. Among the fPAGs, 20 kPa 17% had more integrin positive myofibroblasts than 5kPa ($p < 0.001$), with no differences observed between 5kPa and 8kPa or between 8kPa and 20kPa (Fig. 4c,4d).

3.4 Mechanical cues from substrate stiffness regulate extracellular matrix (ECM) remodeling in Human vaginal fibroblasts

3.4.1 Collagen Deposition

As human vaginal fibroblasts transition to a myofibroblast phenotype, they synthesize and organize a provisional collagen rich matrix. The extent and maturity of this collagen network can therefore serve as a downstream readout of stiffness driven fibroblast activation. Collagen deposition by HvFs cultured on functionalized polyacrylamide gels (fPAGs; 5, 8, and 20kPa) and plain glass slide (PGs) was assessed at days 1, 3, and 7 using Picrosirius Red staining and polarized light microscopy, with color-based pixel segmentation used to calculate the percentage area occupied by red, orange, yellow, and green collagen fibers. Red and orange fibers represent thicker, more mature collagen fibers, whereas yellow and green fibers represent thinner, less organized collagen fibers (Fig. 5a, b). Total collagen deposition, calculated as the sum of the red, orange, yellow, and green collagen fiber positive areas, increased over time and the increase in total collagen deposition was primarily driven by the accumulation of mature (red and orange fiber positive areas) collagen fibers Mean total collagen deposition increased from 33% at day 1 to 61% at day 3 and 91% at day 7 ($p < 0.001$). Relative to day 1, total collagen deposition was 28% greater at day 3 ($p < 0.001$) and 58% higher at day 7 ($p < 0.001$) with a further 30% increase from day 3 to day 7($p < 0.001$). This increase was driven primarily by accumulation of mature (red and orange) fibers as opposed to immature (yellow and green) thinner fibers. Substrate stiffness had a strong effect where relative to PGs, total collagen deposition was 34% greater on the 5kPa ($p = 0.001$), 50% greater on the 8 kPa ($p < 0.001$), and 98% greater on the 20kPa ($p < 0.001$) fPAGs. Among the fPAGs, total collagen deposition was 63% greater on the 20kPa gels than on the 5kPa ($p < 0.001$) and 45% higher than on the 8 kPa ($p = 0.009$) fPAGs, whereas no difference was observed between the 5 and 8kPa fPAGs ($p = 0.215$). Deposition of immature collagen fibers (yellow and green) remained low throughout 7 days of cell

culture and was not affected by time or substrate stiffness. No significant differences were observed across 7 days (all $p > 0.05$), between PG and any of the fPAG (all $p > 0.05$), or among the fPAGs (all $p > 0.05$).

3.4.2 MMP Activity

Beyond depositing collagen, myofibroblasts remodel the matrix they secrete through matrix metalloproteinase (MMP) activity. To determine whether this remodeling capacity is itself stiffness-driven, gelatin zymography was performed on conditioned media collected from hvFs cultured on fPAGs; 5, 8, and 20kPa and plain glass (PG) at days 1, 3, and 7. Gelatinolytic bands corresponding to pro-MMP-2 (~ 72kDa) and active MMP-2 (~ 62kDa) were detected across all substrate conditions and time points (Fig. 6a) and band intensities were quantified by densitometric analysis and normalized to an MMP-9 standard included on each gel to account for inter-gel variability.

Pro-MMP-2 normalized intensity increased significantly over time, rising by 56% at both day 3 ($p = 0.015$) and day 7 relative to day 1 ($p < 0.001$; 20kPa $p = 0.001$). Among the fPAGs, pro-MMP-2 normalized band intensity was 86% higher on the 5kPa than on the 20kPa gels ($p = 0.042$) and 29% higher on the 8kPa than on the 20kPa gels ($p = 0.048$), with no difference observed between the 5kPa and 8kPa gels ($p = 0.125$).

Active MMP-2 normalized band intensity also increased significantly over time, reaching approximately 8-fold and 7-fold higher levels at days 3 and 7, respectively, compared with day 1 (both $p < 0.001$), with no significant difference between days 3 and 7 ($p = 0.485$). Unlike pro-MMP-2, active MMP-2 intensity did not differ significantly from PG on the 5 kPa ($p = 0.745$) or 8 kPa ($p = 0.872$) fPAGs but was significantly higher on the 20 kPa gels ($p = 0.002$). Among the fPAGs, active MMP-2 intensity was approximately 2.25-fold higher on the 20 kPa gels than on either the 5 or 8 kPa gels (both $p = 0.021$), with no significant difference between the 5 and 8 kPa gels ($p = 0.852$) (Fig. 6b).

3.5 TGF-β1 secretion and YAP nuclear translocation reveal a mechanically driven FMT

Transforming growth factor-β1 (TGF-β1) autocrine signaling is a major driver of the fibroblast-to-myofibroblast transition (FMT) in fibrosis. To determine whether the stiffnessinduced FMT observed in this study was associated with biochemical TGF-β1 signaling in addition to mechanical α5 integrin signaling, we quantified total and active TGF-β1 in conditioned media from HvFs across substrate stiffnesses and time points using an enzyme-linked immunosorbent assay (ELISA). Active TGF-β1 remained below the detection limit at all time points, whereas total TGF-β1 secretion increased significantly over time. Compared with day 1, total TGF-β1 was 96.7% higher on day 3 (375.5 pg/mL; $p < 0.001$) and 205.5% higher on day 7 (798.2 pg/mL; $p < 0.001$). On day 7, total TGF-β1 was 55.3% higher than on day 3 (422.8 pg/mL; $p < 0.001$). Substrate stiffness significantly affected total TGF-β1 secretion. Compared with PGs, total TGF-β1 was 36.2% higher on 5 kPa fPAGs (283.0 pg/mL; $p = 0.005$), did not differ significantly on 8-kPa fPAGs (4.6% lower; 36.3 pg/mL; $p = 0.716$), and was 32.9% lower on 20-kPa

fPAGs (257.6 pg/mL; p = 0.010). Among the fPAGs, total TGF-β1 was 42.8% higher on 5-kPa than on 8-kPa fPAGs (319.2 pg/mL; p = 0.001), 103.0% higher on 5-kPa than on 20-kPa fPAGs (540.5 pg/mL; p < 0.001), and 42.2% higher on 8-kPa than on 20-kPa fPAGs (221.3 pg/mL; p = 0.026). TGFBR1 was detectable by immunofluorescence across all substrate conditions, confirming that HvFs retained the receptor machinery necessary for TGF-β1 signaling despite the absence of detectable active ligand (Fig. 7a).

Yes-associated protein (YAP) nuclear-to-cytoplasmic (N/C) ratio at day 1 increased with increasing stiffness (5kPa:1.043; 8kPa: 1.123; 20kPa:1.114, PGs: 1.308; p < 0.01) indicating that early mechanotransduction signaling occurred independent of autocrine TGF-β1 activation (Fig. 7b). This stiffness-dependent YAP response was transient, however decreasing to near baseline levels by day 3 (p = 0.027) through day 7 (p = 0.041), coinciding with a substantial increase in cell density over the same time frame (Table 2). Early YAP nuclear localization converts mechanical cues from substrate stiffness into a transcriptional program. On stiffer substrates, integrin engagement, FAK activation, and RhoA/ROCK-driven cytoskeletal tension promote YAP nuclear entry, where it partners with TEAD transcription factors to regulate genes involved in contractility (ACTA2), matrix remodeling (MMPs), and collagen production. Consistent with mechanotransduction responses, YAP nuclear localization occurred early, preceding αSMA cytoplasmic accumulation, MMP synthesis, and collagen production, consistent with YAP acting as an upstream trigger of the fibroblast-to-myofibroblast transition rather than a consequence of it. The transient YAP response may reflect increased cell-cell contact and reduced spreading at higher cell density, which promotes YAP cytoplasmic retention.

3.6 Substrate Contraction

Having established that stiffer fPAGs mechanically drive greater myofibroblast acquisition, matrix deposition and MMP-2 activity, we probed whether this translated into a proportional increase in a functional output. Traction force microscopy (TFM) was used to measure contractile forces HvFs exert on fPAG substrates across stiffness and time (Fig. 8a, b). At day 1, HVFs generated the greatest traction forces (1050.7 ± 589.8 Pa). By day 3, contractility decreased by 56% (590.9 Pa) relative to day 1 (p < 0.001). Although traction forces remained lower at day 7 compared to day 1, contractility partially recovered, increasing by 69% (318.1 Pa) relative to day 3 (p = 0.008), while remaining 26% (272.7 Pa) below day 1 (p = 0.022). Substrate stiffness also significantly affects traction force generation. Relative to the 5kPa fPAGs, contractility increased by 83% (339.4 Pa) on the 8kPa fPAGs (p = 0.004) and by 177% (722.8 Pa) on the 20kPa fPAGs (p < 0.001). Traction forces were 51% (383.4 Pa) greater on the 20 kPa than on the 8 kPa fPAGs (p = 0.001), demonstrating a progressive increase in contractility with increasing substrate stiffness. This increase in contractility at later time points is consistent with the onset of fibroblast-to-myofibroblast transition (Fig. 4) given that myofibroblasts are known to exert stronger traction forces.

4. DISCUSSION

This study establishes a stiffness-dependent framework for vaginal fibroblast mechanoresponse using polyacrylamide hydrogels covalently conjugated with gelatin via click chemistry (fPAGs) spanning a physiologically and pathologically relevant elastic modulus range (5–20 kPa), benchmarked against a supraphysiologic glass substrate (PG). Mechanical cues have been shown to alter the behavior of fibroblasts from women with POP [14, 19, 20], including changes in integrin expression in premenopausal prolapsed vaginal cells under mechanical loading [20]. However, previous studies captured only part of the response. For example, Ruiz-Zapata et al. measured α-SMA and collagen-gene expression at a single early time point [19], and Gudde et al. studied cells from one patient with POP in a three-dimensional gel without measuring α-SMA or MMP activity [14]. By integrating phenotypic (fibroblast-to-myofibroblast transition, FMT), mechanosensing receptor-level (α5 integrin), matrix-synthesis (collagen deposition), matrix-degradative (MMP-2 activity), and functional (traction force) outcomes, this work provides a multidimensional characterization of how matrix mechanics drive the fibroblast-driven remodeling processes implicated in pelvic organ prolapse (POP) pathophysiology and biomaterial-tissue integration. Collectively, our data demonstrate that increasing substrate stiffness within the physiologically tunable fPAGs drives a coordinated, time-dependent increase in myofibroblast density, integrin engagement, mature collagen deposition, MMP-2 activation, and contractile force generation, with early YAP nuclear localization consistent with a mechanotransductive mechanism, supporting the central hypothesis that matrix rigidity is a key mechanoregulatory determinant of vaginal fibroblast activation state. Cell viability remained ≥ 98% across all substrate conditions and timepoints, confirming that the observed phenotypic and functional divergence reflects substrate-specific mechanotransductive signaling rather than differential cytotoxicity.

4.1 Fibroblast-to-myofibroblast transition is time-dependent

HvFs exhibited a significant, time-dependent increase in α-SMA-positive myofibroblasts, consistent with established models of stiffness-induced myofibroblast differentiation. Critically, this transition occurred against a background of stable total fibroblast density across all timepoints and substrate conditions, indicating that stiffness-driven FMT in this system reflects a genuine phenotypic conversion within a fixed cellular population rather than a confound of proliferation, apoptosis, or differential substrate adhesion. This isolates phenotypic switching as the primary driver of the observed myofibroblast accumulation and parallels ex vivo observations in prolapse-derived vaginal tissue, where elevated stiffness correlates with increased myofibroblast burden and excessive ECM deposition10. These findings establish a quantitative mechanobiological baseline in premenopausal, non-prolapse tissue against which pathological or hormonally altered fibroblast populations can subsequently be benchmarked.

4.2 Alpha 5 (α5) integrin engagement provides a receptor-level substrate for stiffness sensing

α5 integrin was selected as the primary mechanosensitive receptor probed in this study because gelatin which is the ligand used to functionalize the polyacrylamide substrates via copper-catalyzed click chemistry presents RGD-motif binding sites that are preferentially engaged by the α5β1 heterodimer. As one of the principal integrins mediating fibroblast adhesion to RGD-containing ECM ligands, α5β1 was therefore the most direct and substrate-relevant probe for characterizing integrin mediated mechanotransduction in this fPAG system, motivating our focus on this receptor as a mechanistic link between substrate stiffness sensing and downstream FMT. α5 integrin expression provided mechanistic insight into the receptor-level events underlying the human vaginal fibroblasts-to-myofibroblasts transition. Integrin-positive cell density increased progressively with culture duration across all substrates, while the proportion of integrin-positive cells within the total population remained comparatively stable indicating that the dominant driver of this increase was expansion of an integrin engaged subpopulation rather than a uniform shift in per-cell receptor engagement. Stratifying by phenotype clarified this relationship further: the fibroblast-specific integrin-positive fraction remained largely invariant over time, whereas the myofibroblast-specific integrinpositive fraction increased significantly between day 1 and day 3 before reaching a plateau. This pattern indicates that α5 integrin acquisition is preferentially coupled to, and likely contributes to the stabilization of, the myofibroblast phenotype specifically consistent with the established function of the α5β1 heterodimer in mediating focal adhesion formation, cell–ECM force transmission, and mechanosensitive signal transduction during stiffness-driven FMT.

4.3 Stiffness-dependent ECM remodeling reveals a dissociation between phenotype and matrix output on non-tunable substrates

Collagen analysis demonstrated clear time and stiffness dependent increases in mature, type I-like collagen fibers, with maximum accumulation on 20kPa fPAGs. In contrast, immature, type III-like fibers remained minimal, suggesting rapid maturation and remodeling of newly deposited matrix toward a mature collagen phenotype. Such remodeling is consistent with fibrotic tissues, where excessive type I collagen deposition contributes to increased tissue stiffness and progressive loss of normal mechanical function [19]. α5 integrin-positive myofibroblast density was significantly associated with total collagen deposition, although the effect was small (approximately 0.04% per 1,000 cells/mm²; $p = 0.003$). This is consistent with integrin-mediated adhesion supporting matrix deposition and organization, but because both measures increased with culture duration, it should be interpreted as an exploratory association rather than evidence of a direct link. A notable divergence emerged when collagen deposition was compared with myofibroblast phenotype. Despite supporting the highest density of α-SMA-positive cells, PG exhibited the lowest total collagen deposition of all substrates. Several factors may contribute to this dissociation. Unlike the fPAG substrates, glass lacks the compliant and hydrated microenvironment that supports cell-matrix interactions and matrix organization. In addition, differences in collagen retention during Picrosirius Red processing on a nonporous surface cannot be excluded. Regardless of the underlying mechanism, these results suggest that PG is most appropriately used as a control for viability

and phenotypic activation rather than as an extension of the stiffness-response relationship observed across the fPAG stiffnesses. MMP-2 activity revealed a complementary effect of stiffness on matrix remodeling. Activity of MMP-2 was maintained on the 5 and 8 kPa substrates and significantly elevated on 20 kPa fPAGs. The increase in active MMP-2 despite lower levels of its inactive precursor suggests that stiffness influences how matrix-remodeling enzymes are activated rather than simply increasing their overall production. Importantly, these findings indicate that stiffness regulates both matrix deposition and matrix turnover where the stiffest hydrogel simultaneously promoted the greatest accumulation of mature collagen and the highest level of MMP-2 activity. This combination suggests that increased stiffness drives a state of heightened matrix remodeling in which synthesis and degradation occur concurrently. In the context of fibrosis, such behavior may contribute to a self-perpetuating cycle whereby mechanical stiffening stimulates continued matrix reorganization, further reinforcing the fibrotic phenotype.

4.4 Substrate stiffness engages YAP mechanotransduction in the absence of detectable active TGF-β1

Despite robust, stiffness- and time-dependent secretion of latent TGF-β1 and confirmed expression of TGFβR1, active TGF β1 was not detected in conditioned media at any timepoint. These findings suggest that fibroblast-to-myofibroblast transition in this system can occur independently of detectable autocrine TGF-β1 activation. While localized activation of TGF-β1 at the cell surface or within the pericellular matrix cannot be excluded, the absence of measurable active TGF-β1 indicates that canonical soluble TGF-β1 signaling is unlikely to be the primary driver of the stiffness-dependent responses observed in this study. Additional evidence for a TGF-β1-independent mechanism was provided by YAP localization where at day 1, the YAP nuclear-to-cytoplasmic ratio increased with substrate stiffness, indicating that fibroblasts rapidly sensed and responded to the mechanical properties of their environment. This response occurred before substantial extracellular matrix accumulation had developed and in the absence of detectable active TGF-β1, supporting the idea that substrate stiffness can directly engage mechanosensitive signaling pathways. Given the established role of YAP in promoting fibroblast activation and extracellular matrix remodeling, the early increase in nuclear YAP suggests that mechanotransduction may serve as an initiating signal linking matrix stiffness to profibrotic cellular behavior. In the context of fibrosis, this is particularly important because it implies that increasing tissue stiffness can actively reinforce fibroblast activation and matrix remodeling through mechanical signaling pathways. The stiffness-dependent YAP response was transient, returning toward baseline by day 3 through day 7. In contrast, markers of fibroblast activation, including integrin expression, collagen deposition, and MMP-2 activity, continued to increase throughout the culture period. This suggests that YAP may be involved in the initial cellular response to substrate stiffness but is unlikely to fully explain the sustained profibrotic remodeling observed at later stages. Findings from this study demonstrate that substrate stiffness is a major regulator of vaginal fibroblast behavior. Increasing stiffness promoted myofibroblast differentiation, integrin expression, collagen deposition, MMP-2 activation, and cellular contractility, indicating that mechanical cues alone can drive many features of a profibrotic phenotype even in the absence of detectable active TGF-β1.

4.5 Traction force microscopy revealed a biphasic pattern of contractility

Cellular traction forces were highest at day 1, decreased significantly by day 3, and partially recovered by day 7, although they remained below initial levels. Across all timepoints, hvFs cultured on stiffer substrates generated greater forces than those on softer substrates, consistent with enhanced transmission of cell-generated tension in mechanically resistant environments. While α-SMA expression increased throughout the culture period, contractility peaked within the first 24 hours following cell seeding before declining and partially recovering. This pattern suggests that force generation is influenced not only by myofibroblast differentiation but also by the dynamic process of cell-matrix engagement and adaptation. The persistent increase in traction forces on stiffer substrates supports the concept of mechanical feed-forward signaling in fibrosis. As tissues stiffen, resident fibroblasts experience a more mechanically resistant environment that promotes greater force generation, profibrotic activation, and matrix remodeling. These findings suggest that matrix stiffness functions not only as a consequence of fibrotic remodeling but also as a regulator of fibroblast behavior capable of sustaining fibrosis progression.

These observations have important implications for pelvic organ prolapse (POP) repair and biomaterial design. In prolapsed tissue, reduced tissue integrity and altered mechanical properties may impair the normal mechanosensitive signals required for extracellular matrix maintenance. At the opposite extreme, synthetic mesh materials often possess stiffnesses that exceed those of native vaginal tissue and may promote excessive fibroblast activation and matrix remodeling. Our findings suggest that both insufficient and excessive mechanical stimulation may be detrimental, with the latter potentially contributing to the fibrosis, contracture, and tissue complications observed following some mesh based repairs. Rather than maximizing material stiffness, these results support the concept that an optimal mechanical range exists in which fibroblasts can maintain and remodel tissue without entering a pathologic fibrotic state. Identifying this range represents an important goal for the development of next generation of prolapse repair materials. More broadly, the mechanosensitive responses observed in vaginal fibroblasts are consistent with those reported in other fibrotic tissues, suggesting that common mechanobiological principles may regulate fibroblast behavior across organ systems. This study therefore establishes an important baseline for future investigations comparing fibroblasts from postmenopausal and prolapse patients and for the development of patient-specific biomaterial strategies.

LIMITATIONS AND FUTURE DIRECTIONS

The findings establish a mechanobiological baseline but do not capture changes associated with aging, menopause, estrogen deficiency, or prolapse pathology. Future studies should directly compare these populations to determine whether these factors alter stiffness-dependent fibroblast responses. While the fPAG in-vitro model provided precise control over substrate stiffness, it does not reproduce the structural

complexity of native vaginal extracellular matrix. Native tissues contain fibrillar architecture, viscoelastic behavior, and biochemical heterogeneity that are not captured in two-dimensional hydrogel systems. More physiologically representative models, including threedimensional and organotypic culture systems, will be important for determining whether the responses observed here are maintained in a more tissue-like environment.

Finally, the mechanistic analysis was intentionally focused on key markers of mechanotransduction and fibroblast activation. Additional studies examining focal adhesion signaling, downstream mechanotransduction pathways, and broader transcriptional responses will be required to better define how stiffness regulates vaginal fibroblast behavior. Ongoing and future work using bulk RNA sequencing will help identify the molecular programs associated with different stiffness environments and facilitate comparisons among premenopausal, postmenopausal, and prolapse-derived fibroblasts. Incorporation of hormonal modulation and in vivo validation will also be necessary to determine how these findings translate to the clinical setting and to guide the design of improved biomaterials for pelvic floor repair.

Declarations

DISCLOSURES:

The authors declare that they have no known financial or personal relationships that could be viewed as influencing the work presented in this manuscript.

ACKNOWLEDGEMENTS

This work was supported in part by the National Institutes of Health through grant R01

HD083383 awarded to P.A.M. Additional support was provided by the Magee Womens Research Institute Postdoctoral fellowship which provided scholar support for T.O.O. The views expressed in this article are those of the authors and do not necessarily reflect the official policies of the NIH.

DATA AVAILABILITY

The data that supports the findings of this study are available from the corresponding author P.A.M., upon request.

CREDIT EVALUATION:

Temitope Obisesan- Conceptualization, data curation, software, verification, formal analysis, investigation, visualization, writing; Jingnan Ye- data curation, software, formal analysis, visualization, writing; Mya Fulton-data curation, software; Marrisa Therriaultwriting, formal analysis; Katrina Knight-

data curation; Yu Li Wang-project oversight, conceptualization; Pamela Moalli-conceptualization, project overview, funding acquisition, formal analysis, writing.

References

1. Alperin M, Moalli PA. Remodeling of vaginal connective tissue in patients with prolapse. *Curr Opin Obstet Gynecol*. 2006;18(5):544–550. doi:10.1097/01.gco.0000242958.25244.ff. (pubmed.ncbi.nlm.nih.gov)
2. Moalli PA, Shand SH, Zyczynski HM, Gordy SC, Meyn LA. Remodeling of vaginal connective tissue in patients with prolapse. *Obstet Gynecol*. 2005;106(5 Pt 1):953–963. doi:10.1097/01.AOG.0000182584.15087.dd. (pubmed.ncbi.nlm.nih.gov)
3. Wu JM, Matthews CA, Conover MM, Pate V, Jonsson Funk M. Lifetime risk of stress urinary incontinence or pelvic organ prolapse surgery. Obstet Gynecol. 2014 Jun;123(6):1201-1206.https://doi.org/10.1097/AOG.0000000000000286.PMID: 24807341; PMCID: PMC4174312
4. Knight KM, Breedlove S, Obisesan T, et al. Vaginal host response to polycarbonate urethane, an alternative material for the repair of pelvic organ prolapse. *Acta Biomater*. 2024;189:298–310. doi:10.1016/j.actbio.2024.09.040. (pmc.ncbi.nlm.nih.gov)
5. Jones KA, Feola A, Meyn L, Abramowitch SD, Moalli PA. Tensile properties of commonly used prolapse meshes. Int Urogynecol J. 2009;20:847–853. doi:10.1007/s00192-008-0781-x.
6. Dub25 Dubik J, Alperin M, De Vita R. The biomechanics of the vagina: a complete review of incomplete data. npj Womens Health. 2025. doi:10.1038/s44294-02400047-7.
7. Thunes JR, Pal S, Moalli P, Abramowitch S, Maiti S. Mismatches in stiffness between the vagina and transvaginal mesh lead to stress concentrations near an anterior wall incision. *ASME 2013 Summer Bioengineering Conference*. 2013. doi:10.1115/SBC2013-14688
8. Liang R, Abramowitch S, Knight K, Palcsey S, Nolfi A, Feola A, Stein S, Moalli P. Vaginal degeneration following implantation of synthetic mesh with increased stiffness. BJOG 2013; 120: 233–243. https://doi.org/10.1111/1471-0528.12085
9. Feola A, Abramowitch SD, Jallah Z, et al. Deterioration in biomechanical properties of the vagina following implantation of a high stiffness prolapse mesh. *BJOG*. 2013;120(2):224–232. doi:10.1111/1471-0528.12077
10. Knight KM, King GE, Palcsey SL, Suda A, Liang R, Moalli PA. Mesh deformation: a mechanism underlying polypropylene prolapse mesh complications in vivo. *Acta Biomater*. 2022;148:323 -335. doi:10.1016/j.actbio.2022.05.05
11. Humphrey, J., Dufresne, E. & Schwartz, M. Mechanotransduction and extracellular matrix homeostasis. *Nat Rev Mol Cell Biol***15**, 802–812 (2014). https://doi.org/10.1038/nrm3896
12. D'Urso M and Kurniawan NA (2020) Mechanical and Physical Regulation of Fibroblast–Myofibroblast Transition: From Cellular Mechanoresponse to Tissue Pathology. Front. Bioeng. Biotechnol. 8:609653. d https://www.frontiersin.org/journals/bioengineering-

andbiotechnology/articles/10.3389/fbioe.2020.609653. JOURNAL=Frontiers in Bioengineering and Biotechnology. Volume 8 – 2020. DOI=10.3389/fbioe.2020.609653. ISSN=2296-4185.

13. Z. Chen, M. Ezzo, B. Zondag, F. Rakhshani, Y. Ma, B. Hinz, E. Kumacheva, *Intrafibrillar Crosslinking Enables Decoupling of Mechanical Properties and Structure of a Composite Fibrous Hydrogel*. *Adv. Mater.* 2024, 36, 2305964. https://doi.org/10.1002/adma.202305964
14. Aksel N. Gudde, Melissa J. J. van Velthoven, Betül Türkel, Paul H. J. Kouwer, JanPaul W. R. Roovers, Zeliha Guler; Vaginal Fibroblast Behavior as a Function of Stiffness Changes in a Polyisocyanide Hydrogel for Prolapse Repair. *ACS Appl. Bio Mater.* 18 September 2023; 6 (9): 3759–3767. https://doi.org/10.1021/acsabm.3c00433
15. Merkt W, Zhou Y, Han H, Lagares D. *Myofibroblast fate plasticity in tissue repair and fibrosis: Deactivation, apoptosis, senescence and reprogramming*. *Wound Rep Reg*. 2021; 29: 678–691. https://doi.org/10.1111/wrr.12952
16. Hinz, B., Lagares, D. Evasion of apoptosis by myofibroblasts: a hallmark of fibrotic diseases. *Nat Rev Rheumatol***16**, 11–31 (2020). https://doi.org/10.1038/s41584-019-0324-5. Accepted04 October 2019.
17. S. Asano, S. Ito, K. Takahashi, K. Furuya, M. Kondo, M. Sokabe, Y. Hasegawa. *Matrix stiffness regulates migration of human lung fibroblasts*. *Physiol Rep*, 5 (9), 2017, e13281, https://doi.org/10.14814/phy2.13281
18. Wang H, Haeger SM, Kloxin AM, Leinwand LA, Anseth KS (2012) Redirecting Valvular Myofibroblasts into Dormant Fibroblasts through Light-mediated Reduction in Substrate Modulus. PLOS ONE 7(7): e39969. https://doi.org/10.1371/journal.pone.0039969
19. Ruiz-Zapata, A.M.; Heinz, A.; Kerkhof, M.H.; van de Westerlo-van Rijt, C.; Schmelzer, C.E.H.; Stoop, R.; Kluivers, K.B.; Oosterwijk, E. Extracellular Matrix Stiffness and Composition Regulate the Myofibroblast Differentiation of Vaginal Fibroblasts. Int. J. Mol. Sci. 2020, 21, 4762. https://doi.org/10.3390/ijms21134762
20. Kufaishi H, Alarab M, Drutz H, Lye S, Shynlova O. Static mechanical loading influences the expression of extracellular matrix and cell adhesion proteins in vaginal cells derived from premenopausal women with severe pelvic organ prolapse. *Reprod Sci*. 2016;23(7):978–992. doi:10.1177/1933719115625844
21. Yeung, T., Georges, P.C., Flanagan, L.A., Marg, B., Ortiz, M., Funaki, M., Zahir, N., Ming, W., Weaver, V. and Janmey, P.A. (2005), Effects of substrate stiffness on cell morphology, cytoskeletal structure, and adhesion. Cell Motil. Cytoskeleton, 60: 24-34. https://doi.org/10.1002/cm.20041
22. Gałdyszyńska M, Bobrowska J, Lekka M, et al. *The stiffness-controlled release of interleukin-6 by cardiac fibroblasts is dependent on integrin α2β1*. *J Cell Mol Med*. 2020; 24: 13853–13862. https://doi.org/10.1111/jcmm.15974
23. Tse, J. R., & Engler, A. J. (2010). Preparation of hydrogel substrates with tunable mechanical properties. Current Protocols in Cell Biology, 47(1), https://doi.org/10.1002/0471143030.cb1016s47

24. Vu Hong, Nicole F. Steinmetz, Marianne Manchester, M. G. Finn; Labeling Live Cells by Copper-Catalyzed Alkyne–Azide Click Chemistry. *Bioconjugate Chem.* 20 October 2010; 21 (10): 1912–1916. https://doi.org/10.1021/bc100272z
25. Invitrogen. (2005). LIVE/DEAD® Viability/Cytotoxicity Kit for mammalian cells: Product information sheet (MP 03224). Molecular Probes, Inc. https://www.thermofisher.com/order/catalog/product/L3224
26. Hu, X., Beeton, C. Detection of Functional Matrix Metalloproteinases by Zymography. J. Vis. Exp. (45), e2445, doi:10.3791/2445 (2010).
27. Thermo Fisher Scientific. *Novex Pre-Cast Gel Electrophoresis Guide: General Information and Protocols for Using Novex Pre-Cast Gels.* User Guide, Pub. No. MAN0003187, Rev. A.0; 2020. Novex Pre-Cast gel electrophoresis guide User Guide (Pub.No. MAN0003187 A.0)
28. Yu-li Wang, Yun-Chu Lin. Traction force microscopy by deep learning. Biophysical Journal, Volume 120, Issue 15, 2021, Pages 3079-3090, ISSN 0006-3495, https://doi.org/10.1016/j.bpj.2021.06.011

Figures

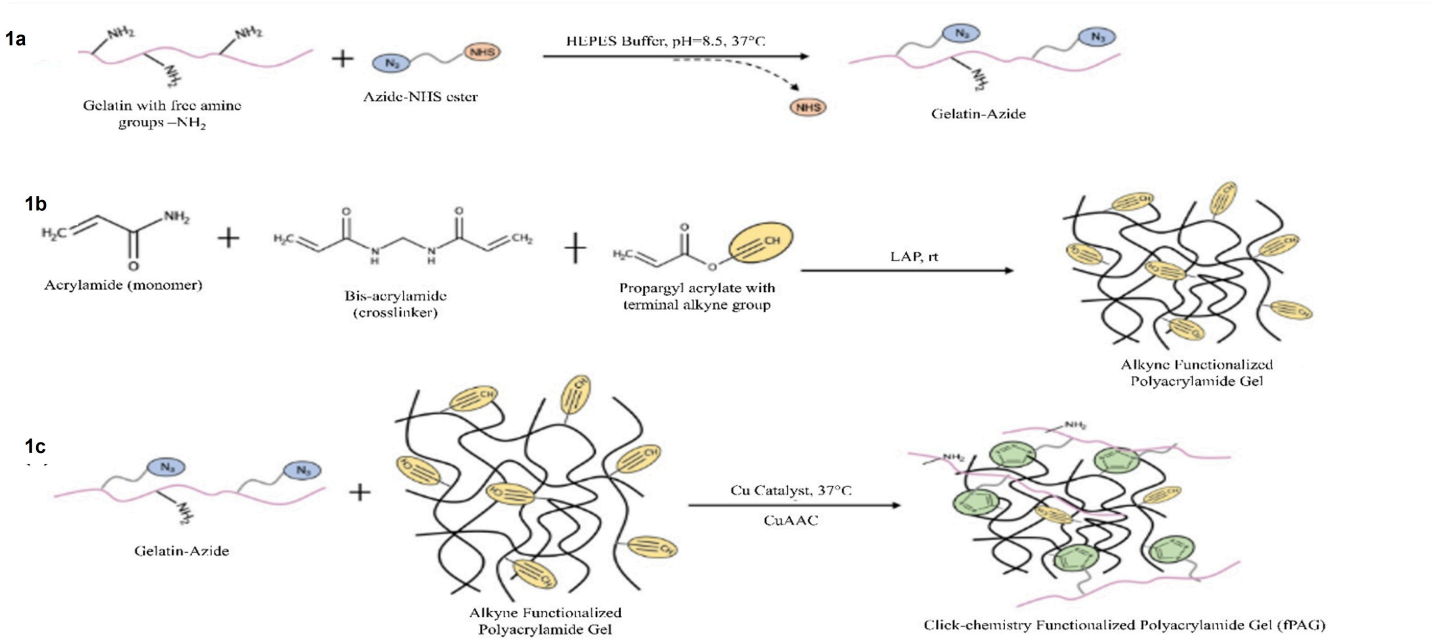


Figure 1

Gelatin-azide was conjugated via copper-catalyzed azide-alkyne click chemistry, enabling covalent attachment of an ECM-mimetic ligand to the polyacrylamide gels. Click chemistry functionalization proceeded in three steps: gelatin was first converted to an azide-bearing form, polyacrylamide gels were separately functionalized with alkyne groups, and the two components were then joined via click chemistry to produce the final conjugated substrate.

(a) Gelatin's free amine groups ($-NH_2$) reacted with an azide-NHS ester in HEPES buffer (pH 8.5, 37°C), covalently linking azide groups to the gelatin backbone via NHS-ester amine coupling and releasing NHS as a byproduct, yielding gelatin-azide.

(b) Acrylamide monomer, bis-acrylamide crosslinker, and propargyl acrylate (bearing a terminal alkyne group) were co-polymerized under UV light with lithium phenyl-2,4,6-trimethylbenzoylphosphinate (LAP) photoinitiator at room temperature, producing an alkyne-functionalized polyacrylamide (PA) gel with alkyne groups displayed throughout the polymer network.

(c) Gelatin-azide was then reacted with the alkyne-functionalized PA gel via copper-catalyzed azide-alkyne cycloaddition (CuAAC; Cu catalyst, 37°C), covalently conjugating gelatin to the gel through triazole linkages and yielding the final click-chemistry modified gelatin-PA gel.

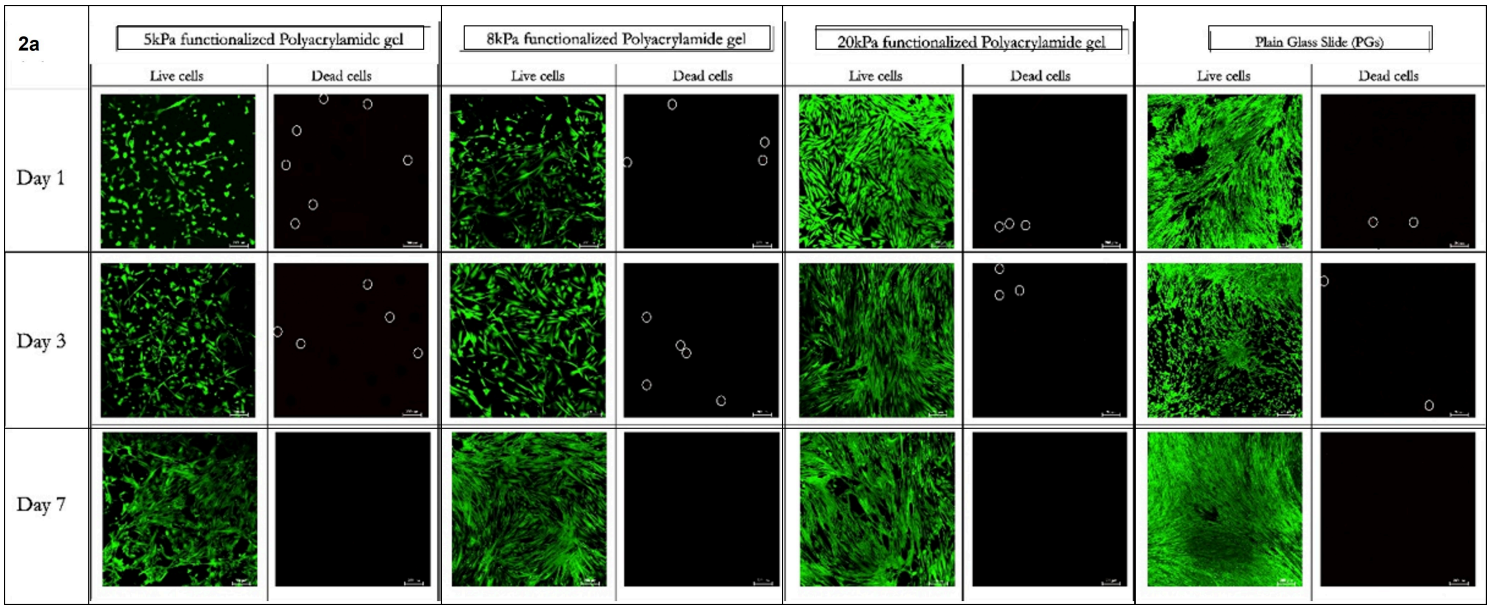


Figure 2

High cell viability across substrate stiffness and culture time. Human vaginal fibroblasts were cultured on functionalized polyacrylamide gels of varying stiffness (5kPa, 8kPa, 20kPa) or on plain glass slides (PGs) and assessed for viability at days 1, 3, and 7 using a live/dead fluorescence assay.

(a) Representative immunofluorescence images show live cells (FITC, green channel) and dead cells (TRITC, red channel, with sparse dead cells circled in white for visibility) across all stiffness conditions and timepoints, consistent with the high viability seen quantitatively in Fig. 2b. Images were acquired at 20X objective using the FITC and TRITC channels, and cells were counted in QuPath.

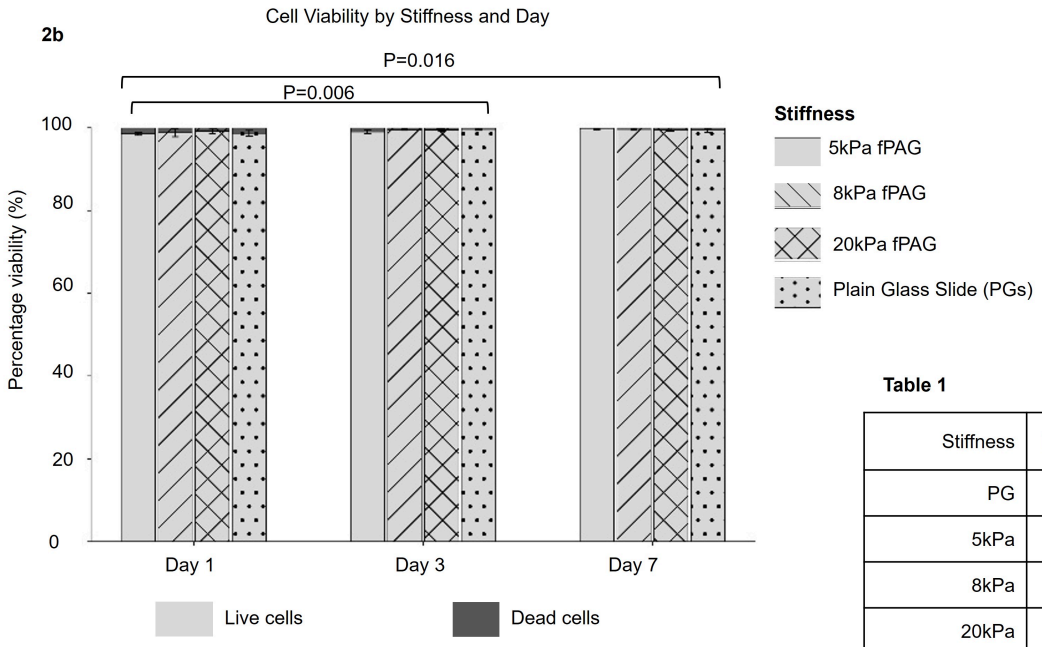


Table 1

Stiffness	Mean (SD)	Mean Difference (95% CI)	P-value
PG	99.2 (0.6)	Referent	
5kPa	99.1 (0.6)	-0.12 (-0.53, 0.29)	.559
8kPa	99.3 (0.7)	0.10 (-0.23, 0.43)	.546
20kPa	99.4 (0.5)	0.20 (0.16, 0.24)	<.001
5kPa vs 8kPa		-0.22 (-0.33, -0.11)	<.001
5kPa vs 20kPa		-0.32 (-0.69, 0.05)	.094
8kPa vs 20kPa		-0.10 (-0.39, 0.19)	.511

Figure 3

Fig. 2b. Stacked bar graph shows maximal viability as culture time progressed, with increased cell viability at days 3 and 7 compared to Day 1 (P=0.006 and P=0.016, respectively), though viability plateaued between day 3 and day 7 (P=0.115), with no further significant change. Stiffness is denoted by pattern on the bars (plain, diagonal, cross-hatch, and dotted for 5kPa, 8kPa, 20kPa, and PG, respectively); live and dead cells are shown in light and dark gray. Error bars represent SD.

Table 1 shows substrate stiffness had little to no effect on viability, as viability exceeded 98% across all stiffness conditions relative to the plain glass slide control.

P-value from mixed-effects general linear regression. Statistical significance was set at P<0.05.

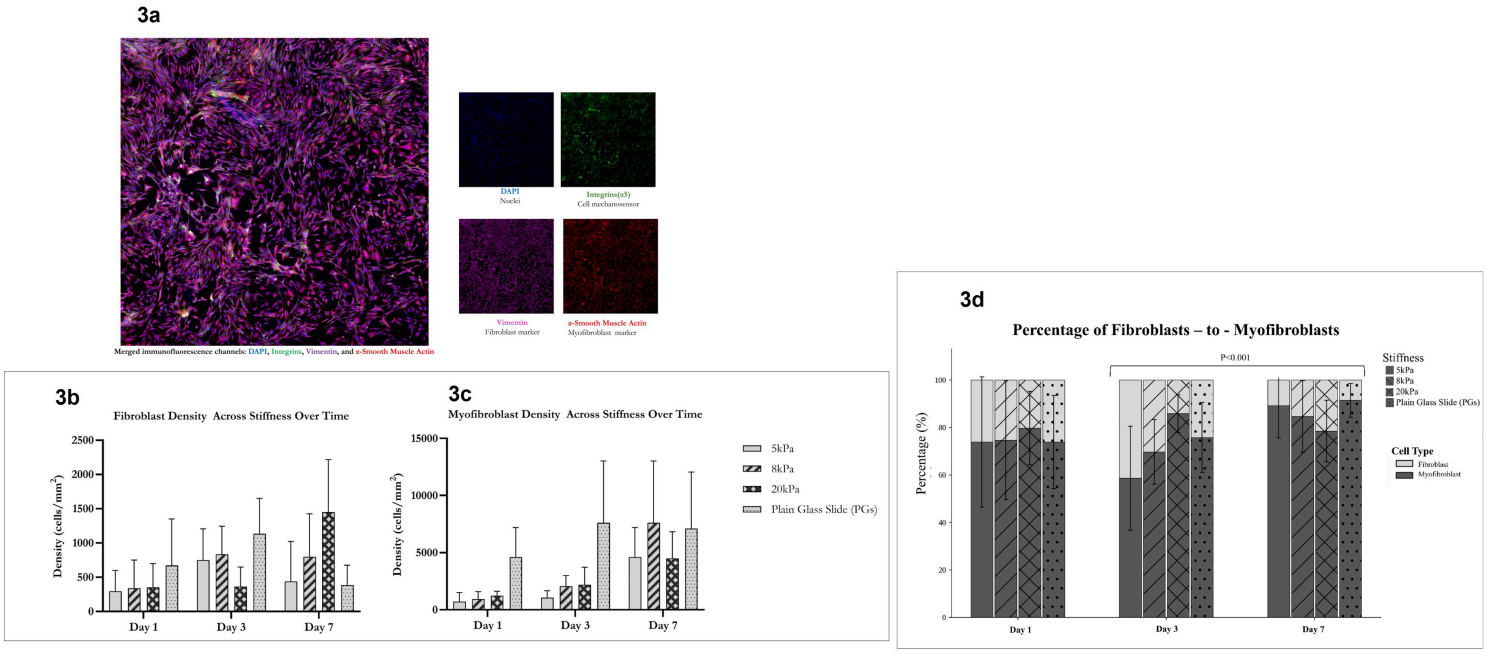


Table 2

	Fibroblast density (cells/mm²)		P-value	Myofibroblast density (cells/mm²)		P-value	Percentage of Fibroblasts (%)		P-value	Percentage of Myofibroblasts (%)		P-value
Plain Glass Slide (PGs)	731	Referent		4370	Referent		20	Referent		81	Referent	
5kPa	496	-236	0.43	2128	-2243	<0.001	27	7	0.60	73	-8	0.47
8kPa	658	-73	0.41	3537	-834	0.39	24	4	0.042	77	-4	0.04
20kPa	722	-9	0.97	3446	-925	<0.001	19	-1	0.84	82	1	0.84
5kPa vs. 8kPa		-166	0.66		-1409	0.08		2	0.87		-4	0.76
5kPa vs. 20kPa		-227	0.22		-1318	<0.001		8	0.37		-9	0.18
8kPa vs. 20kPa		-64	0.84		92	0.92		5	0.45		-5	0.45

Figure 4

Fig. (3a) Representative immunofluorescence images of gels across timepoints acquired at 20X objective show merged channels alongside individual channels: DAPI (nuclei), TRITC (α-smooth muscle actin, myofibroblast marker), and CY5 (vimentin, fibroblast marker).

Fig. (3b) Fibroblast density remained low and variable across all stiffness and timepoints, with no significant differences by culture day (P=0.305) or substrate stiffness (all pairwise P>.05; see **Table 2**).

Fig. (3c) Myofibroblast density, in contrast, increased roughly six-folds from day 1 to day 7. This time-dependent rise was consistent and significant across all three pairwise day comparisons (**Table 2**). Stiffness had a more limited effect: myofibroblast density was significantly lower on 5kPa compared to both PG (P<.001) and 20kPa (P<.001), but with no difference between other stiffnesses.

Fig. (3d) The phenotypic transition between the two populations is captured directly by the percentage of fibroblasts relative to myofibroblasts (%FMT). Myofibroblasts made up majority of cells at every timepoint and stiffness, and this dominance increased with time (P<.001).

Stiffness is denoted by pattern (plain, diagonal, cross-hatch, and dotted for 5kPa, 8kPa, 20kPa, and PG, respectively). Error bars represent SD.

Table 2 shows mean fibroblast density, myofibroblast density, and percentages of fibroblasts and myofibroblasts by substrate stiffness. Values are means for 5kPa, 8kPa, and 20kPa functionalized polyacrylamide gels and plain glass slides (PGs). Differences are relative to PGs (referent) or between the stiffnesses indicated.

P-values are from a mixed-effects linear regression model, and significance was set at P<0.05

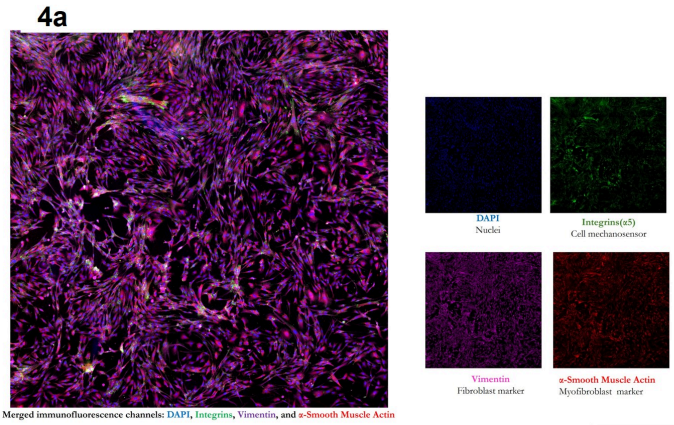
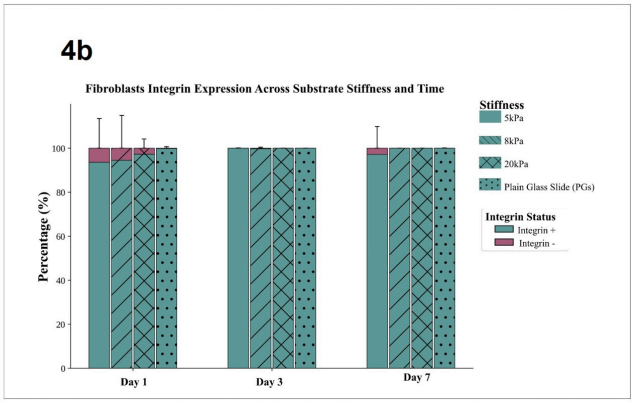
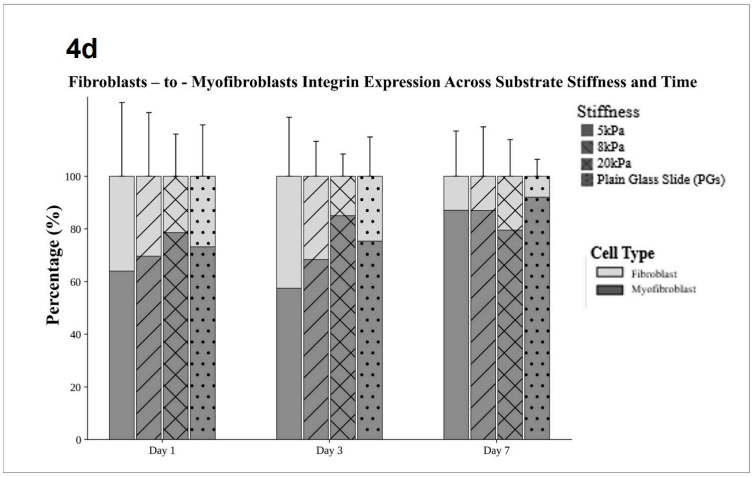


Table 3

Density of cells expressing integrins (cells/mm²)			
Day			P-value
1	1334	Referent	
3	3095	1761	<.001
7	6506	5172	<.001
3 vs7		-3412	0.05
Stiffness			P-value
PG	5014	Referent	
5kPa	2274	-2740	<.001
8kPa	3277	-1737	0.01
20kPa	4015	-999	<.001
5k vs 8k		-1003	<.001
5k vs 20k		-1741	0.002
8k vs 20k		-738	0.31





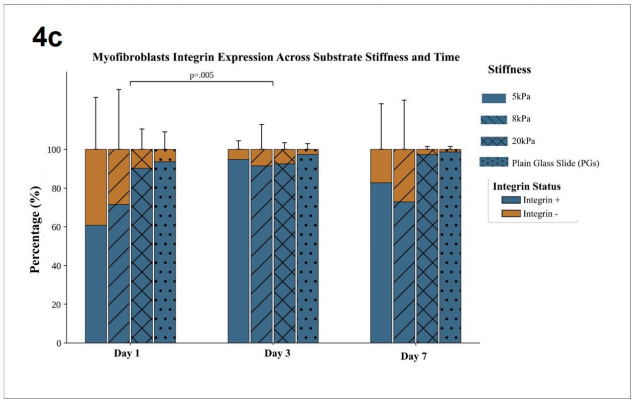


Figure 5

Fig. 4. Matrix stiffness regulates α5 integrin acquisition over time.

(4a) Representative 20X merged and single-channel immunofluorescence images of HvFs showing DAPI (nuclei), α5 integrin, vimentin, and α-SMA; scale bar = [X] μm.

(4b) Percentage of α5 integrin-positive and integrin-negative fibroblasts (DAPI+/vimentin+/α-SMA−) across stiffness and time.

(4c) Percentage of α5 integrin-positive and integrin-negative myofibroblasts (DAPI+/vimentin+/α-SMA+); bracket indicates day 1 vs day 3 (p=0.005).

(4d) Relative proportions of fibroblasts and myofibroblasts, expressed as percentages of α5 integrin-positive cells, across stiffness and time.

Table 3 reports α5 integrin-positive cell density (cells/mm²) as model estimates averaged across days or stiffnesses. Stiffness is denoted by pattern (plain, diagonal, cross-hatch, and dotted for 5 kPa, 8 kPa, 20 kPa, and PG, respectively). Bars show mean ± SD (N=3 donors, n=2 gels per donor). Statistical analysis used mixed-effects linear regression.

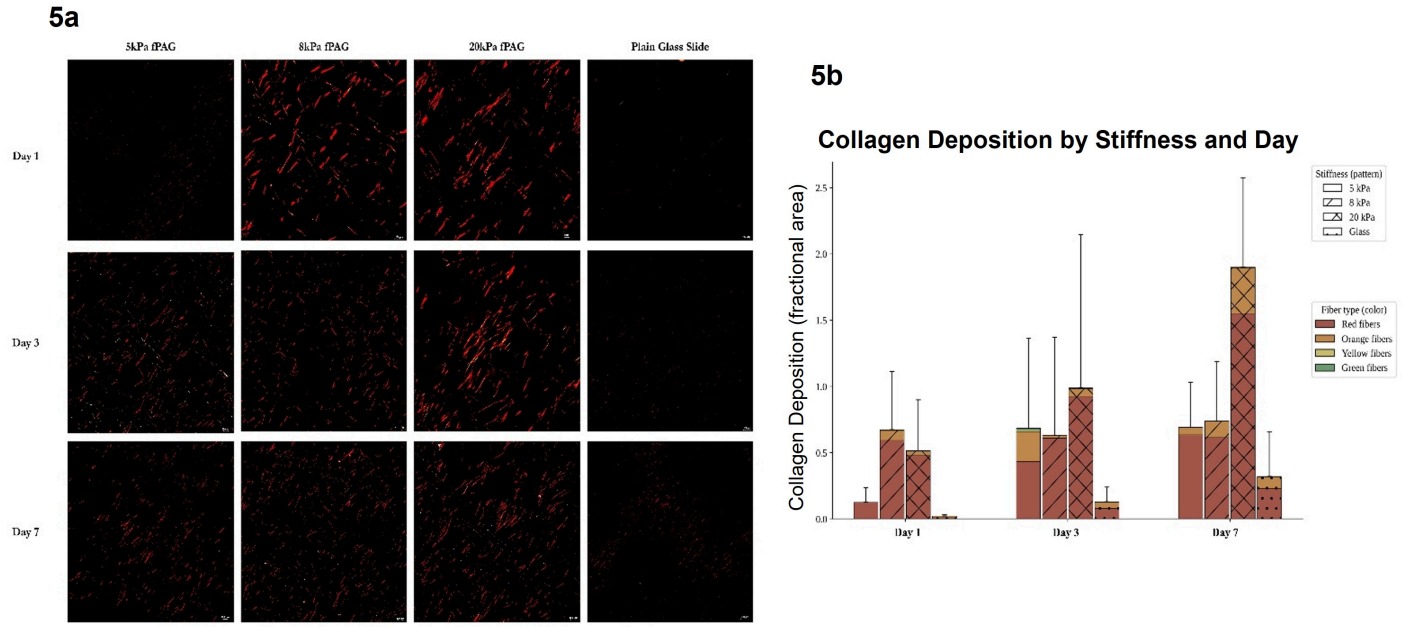


Figure 6

Fig. 5. Matrix stiffness regulates collagen deposition over time.

(5a) Representative Picrosirius Red images under polarized light (10X) of HvFs cultured on 5, 8, and 20 kPa fPAGs and plain glass (PG) at days 1, 3, and 7; scale bar = [X] μm.

(5b) Stacked bar graph of collagen fiber area (% of imaged area) by birefringence color: red and orange (thicker, mature fibers) and yellow and green (thinner, less organized fibers).

Stiffness is denoted by pattern (plain, diagonal, cross-hatch, and dotted for 5 kPa, 8 kPa, 20 kPa, and PG, respectively). Bars show mean ± SD (N=3 donors, n=2 gels per donor). Statistical analysis used mixed-

effects linear regression.

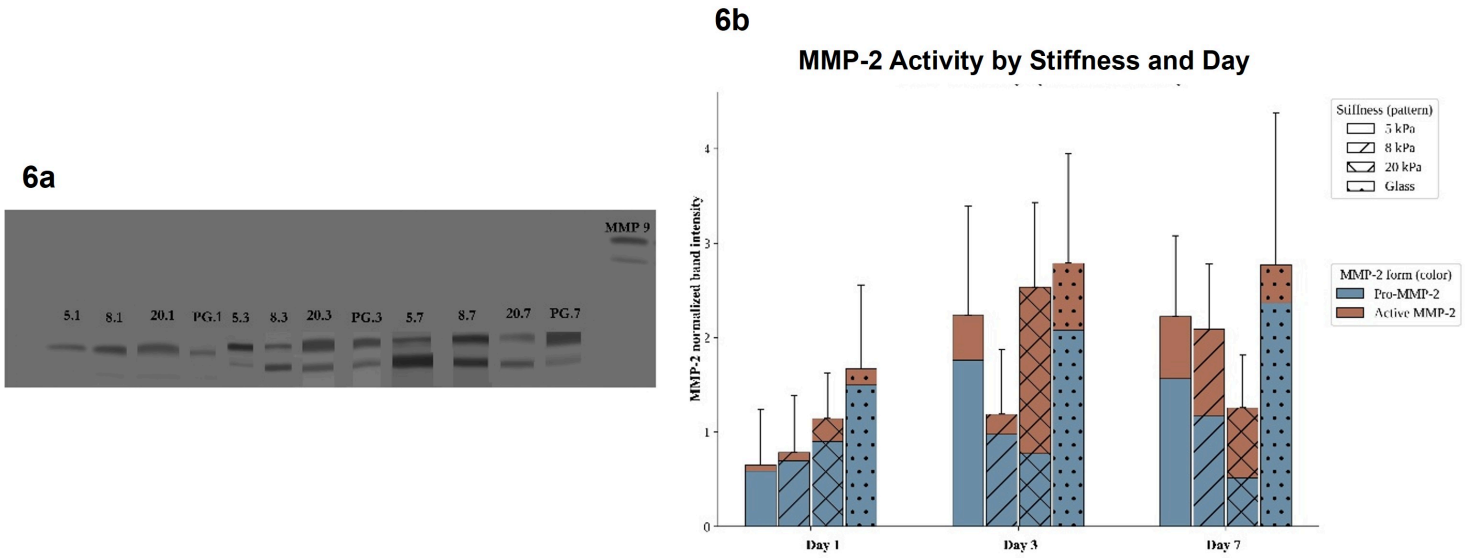


Figure 7

Fig. 6. Matrix stiffness regulates MMP-2 activity over time.

(6a) Representative gelatin zymogram of conditioned media from HvFs cultured on 5, 8, and 20 kPa fPAGs and plain glass (PG) at days 1, 3, and 7, showing pro-MMP-2 (~72 kDa) and active MMP-2 (~62 kDa) bands. Lane labels give stiffness (kPa) and day (e.g., 5.1 = 5 kPa, day 1); MMP-9 (92 kDa) was used as the normalization standard. **(6b)** Stacked bar graph of pro-MMP-2 and active MMP-2 band intensities, normalized to the MMP-9 standard. Stiffness is denoted by pattern (plain, diagonal, cross-hatch, and dotted for 5 kPa, 8 kPa, 20 kPa, and PG, respectively). Bars show mean ± SD (N=3 donors, n=2 gels per donor). Statistical analysis used mixed-effects linear regression.

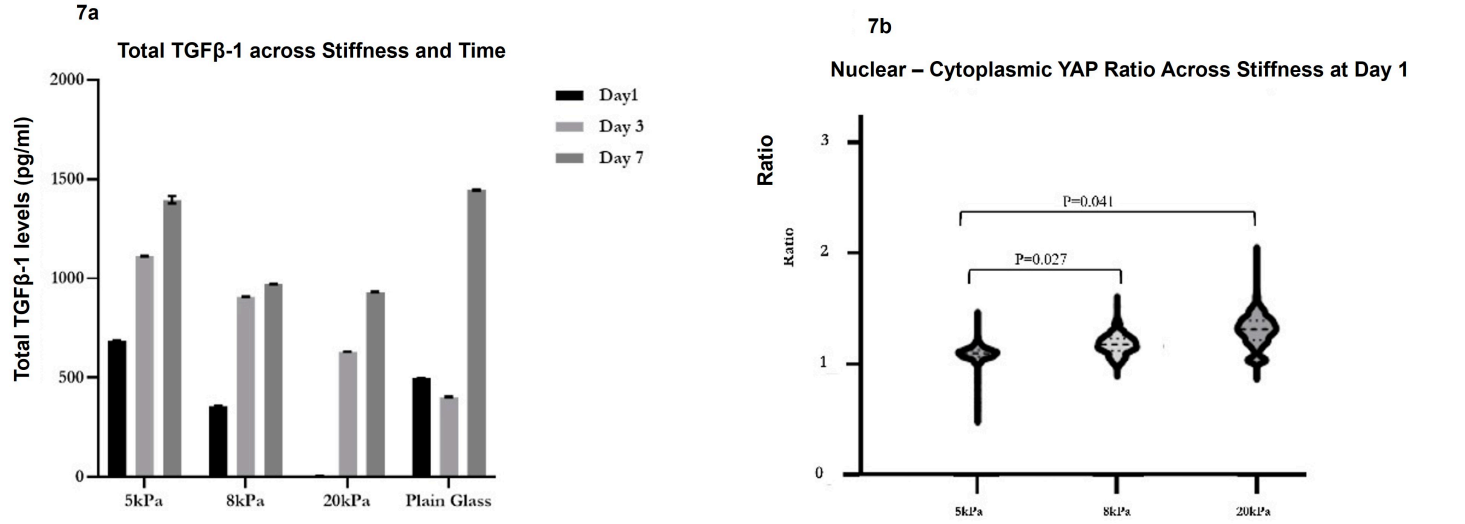


Figure 8

Fig. 7. Total TGF-β1 secretion and early YAP nuclear localization across substrate stiffness.

(7a) Total TGF-β1 (pg/mL) in conditioned media of HvFs cultured on 5, 8, and 20 kPa fPAGs and plain glass (PG) at days 1, 3, and 7. Active TGF-β1 was below the detection limit at all timepoints. Bars show mean ± SD (N=3 donors, n=2 gels per donor).

(7b) Nuclear-to-cytoplasmic (N/C) YAP intensity ratio in HvFs on 5, 8, and 20 kPa fPAGs at day 1. Violin plots show the distribution of single-cell ratios; dashed lines indicate the median and quartiles. Brackets indicate significant pairwise comparisons.

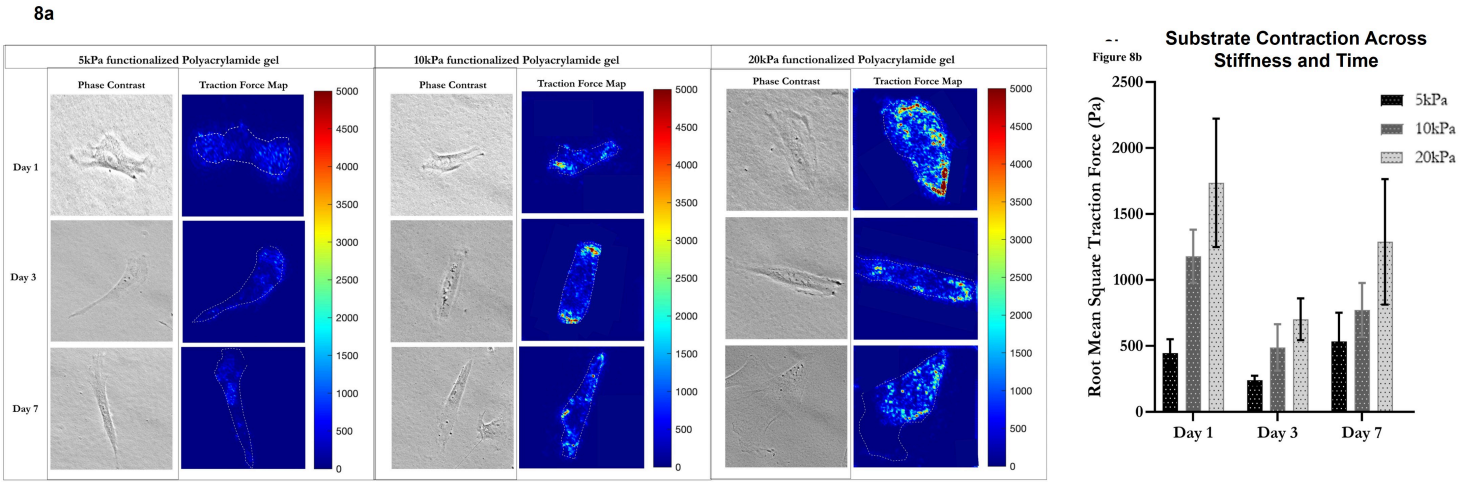


Figure 9

Fig. 8a: Representative phase-contrast images and corresponding traction force heat maps of individual human vaginal fibroblasts cultured on functionalized polyacrylamide gels of 5, 10 and 20kPa stiffness. The color gradient represents magnitude of traction forces with lower forces shown in blue and progressively higher forces represented by green, yellow, and red.

Fig. 8b: Quantification of traction force is shown as root mean square (RMS) traction force (Pa) across 7 days